SCIENCE CHINA
Information Sciences

• RESEARCH PAPER •

April 2020, Vol. 63 140304:1–140304:10
https://doi.org/10.1007/s11432-019-2800-0

Special Focus on Deep Learning in Remote Sensing Image Processing

Deep-learning-based extraction of the animal migration patterns from weather radar images

Kai CUI[1,2], Cheng HU[1,2], Rui WANG[1,2*], Yi SUI[1,2], Huafeng MAO[1,2] & Huayu LI[1,2]

[1]*Radar Research Laboratory, School of Information and Electronics, Beijing Institute of Technology, Beijing* 100081*, China;*
[2]*Key Laboratory of Electronic and Information Technology in Satellite Navigation (Beijing Institute of Technology), Ministry of Education, Beijing* 100081*, China*

Received 31 October 2019/Revised 6 January 2020/Accepted 16 February 2020/Published online 9 March 2020

Abstract Continental coverage and year-round operation of the weather radar networks provide an unprecedented opportunity for studying large-scale airborne migration. The broad and local-scale airborne information collected by these infrastructures can answer many ecological questions. However, extracting and interpreting the biological information from such massive weather radar data remains an intractable problem. Recently, many big-data problems have been solved using the deep learning technology. In this study, the biological information in the weather radar data is identified using the advanced deep learning method. The proposed method consists of two main parts, i.e., a rendering and casting procedure and an image segmentation procedure based on a convolutional neural network. The biological data are automatically extracted by rendering and mapping, image segmentation, and result masking. By analyzing the typical radar data from single and multiple stations, we partly reveal the intensity and speed of the migration pattern. We present the first feasibility study of the extraction of local and large-scale biological phenomena from the Chinese weather radar network data.

Keywords weather radar, deep learning, aerial animal, migration pattern, Chinese weather radar network

Citation Cui K, Hu C, Wang R, et al. Deep-learning-based extraction of the animal migration patterns from weather radar images. Sci China Inf Sci, 2020, 63(4): 140304, https://doi.org/10.1007/s11432-019-2800-0

1 Introduction

The weather radar networks have proved to be invaluable in the studies of airborne animal movements [1, 2]. These radar data can quantify flying animals over a large coverage area [3], providing an unprecedented opportunity for analyzing the long-term changes in their numbers [4]. A detailed analysis of networked radar data can answer biological and ecological questions, such as the vertical structure [5] and flight orientation [6] of the target animals. Although weather radar facilitates collective monitoring, dedicated high-resolution radars are required for meticulous individual observations, including species identification, orientation, and airspeed estimation [7–10].

We seek to answer the biological questions by analyzing the weather radar data. Radar data contain clear visual patterns that can be screened for biological phenomena. However, identifying the biological echoes among the huge volume of weather radar is almost impossible for humans. Deep learning has revolutionized the accuracy of computational tasks with respect to images as well as video and audio data [11]. Combined with the deep learning technique, the weather radar data are a valuable source of aerial animal movements [12–14]. Although good results have been achieved in the United States

* Corresponding author (email: bit.wangrui@gmail.com)

and Europe, related work on Chinese weather radar has not yet been reported. As China currently lacks a wide range of operational dual-polarization weather radar networks, we attempt to mine valuable biological information from the historical Chinese single-polarization radar data.

The main contributions of this study are listed as follows.

- We discuss the geometry of the weather radar biological observations and reveal the difference between the normal meteorological echoes and the biological echoes. We then relate the animal movements to the radar measurements.
- We propose a biological echo extraction technique that retrieves large-scale aerial animal movements. By rendering the radar data as images, we convert the echo extraction problem into an image segmentation task. The segmentation is automated using a modified convolutional neural network (CNN).
- Applying the proposed method to the Chinese weather data, we analyze two migration cases. We demonstrate, for the first time, that local-scale and large-scale biological phenomena can be extracted from the Chinese weather radar network data.

The remainder of this paper is structured as follows. Section 2 explains the observation geometry and echo extraction technique of the proposed method. Section 3 demonstrates our method with respect to the Chinese weather radar data. This study concludes in Section 4.

2 Methods

To unearth the potential of biological monitoring in weather radar data, we need to investigate how weather radar observes the atmosphere and how biological information can be extracted from the data. This section discusses the observation geometry and the strategy of scanning the weather radar, including the products and the data rendering process. Finally, it describes and analyzes the biological echo extraction process based on the CNN technique.

2.1 Radar data

An operational radar network of over 200 Doppler weather radars in China, called the China next generation weather radar (CINRAD) network, is crucial for monitoring large-scale airspaces [15, 16]. To extract biological phenomena from weather radar data, the observation geometry must be dissected. The radar data products of biological and meteorological echoes are obviously distinguished by the spatial distribution difference between the precipitation and aerial animal phenomena. To apply the commonly used image segmentation method, the polar gridded data are rendered into a Cartesian gridded image.

2.1.1 *Observation geometry and scanning strategy*

Most Chinese weather radars are horizontally polarized Doppler radars with a nominal 3-dB beamwidth of 1°. They sample the surrounding airspace in plan position indicator (PPI) scan mode. A weather radar data product is stored as a set of sweeps. Each sweep is recorded in polar grid form, with each azimuth θ represented by approximately 360 range vectors. In the default volume coverage pattern, the radars provide PPI sweeps with elevation angles ranging from 0.5° to 19.5° at 6-minute intervals. As the radar beam is approximately 1° wide, the lowest elevation 0.5° returns the information between 0° and 1° above the horizon. To improve their volume coverage, radar scans are designed to increment their elevation by approximately one-degree intervals. Figure 1 overviews the geometry of weather radar observations and shows the typical volume coverage pattern.

2.1.2 *Data products and rendering*

Single polarized weather radars have three meteorological base-data quantities: the reflectivity factor, the mean radial velocity, and the spectrum width. The data are collected and recorded in units of files, which typically contain six minutes of base data in the normal volume coverage pattern. The radar reflectivity factor data represent the echo intensity in each sampling volume, which is usually recorded in decibels

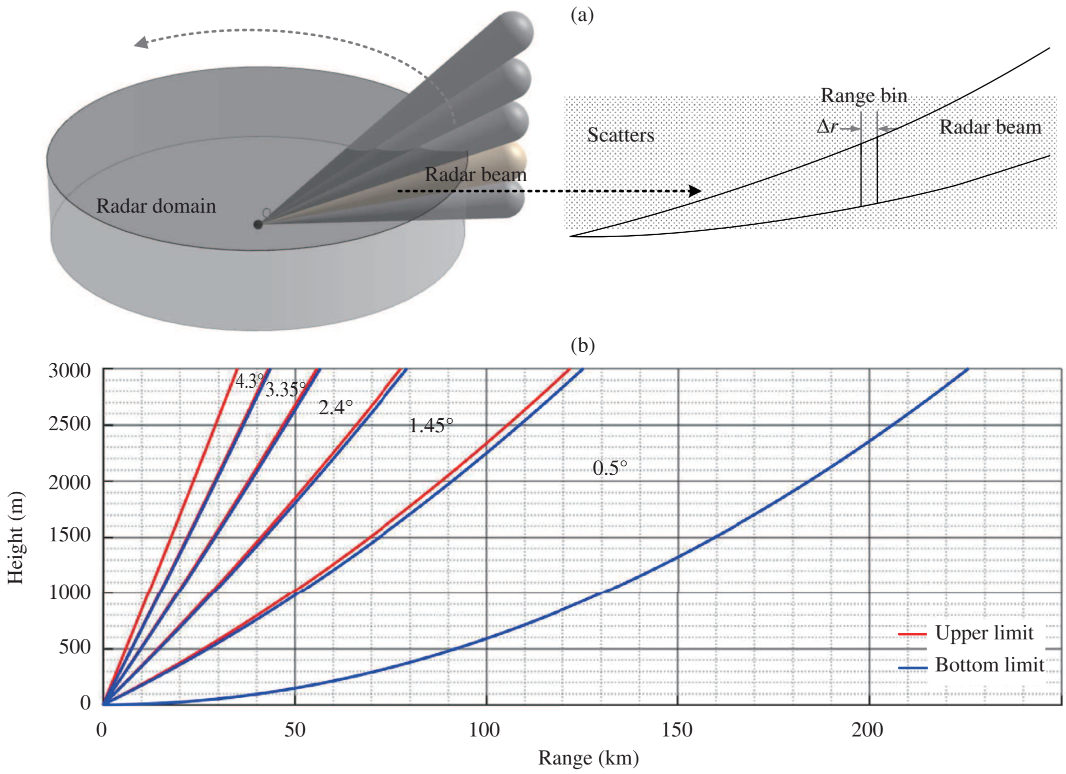

Figure 1 (Color online) Geometry and volume coverage pattern of weather radar scanning. (a) Scanning strategy and beam geometry of normal weather radar. Five successive elevations are shown. (b) Volume coverage patterns at operational elevations of 0.5°, 1.45°, 2.4°, 3.35°, and 4.3°. When two adjacent elevations overlap, the beams scan the atmosphere with no gap between those elevations.

(dBZ) [3]. This quantity was chosen for discriminating the echo types because it distinctly characterizes the precipitation and biological echoes, as highlighted as follows.

- Precipitation has a much higher echo top than biology. Most of the precipitation echoes vertically extend to thousands or even tens of thousands of meters. Cloud microphysical processes occur inside clouds, which are affected by temperature, atmospheric pressure, humidity, and other altitude-related physical parameters. Internal cloud temperatures can be as low as −20°C, meaning that cloud tops can reach 10000 m [17]. Aerial animals cannot tolerate such low temperatures, and most of them fly below 3000 m [18].
- The maximum intensity of precipitation is much higher than that of biology. The maximum intensity can exceed 50 dBZ for precipitation echoes, but rarely exceeds 20 dBZ for biological echoes [19].
- Precipitation and biology have different spatial distributions. Precipitation is greatly affected by the underlying surface and the intensity of the precipitation echoes varies widely within the radar domain. In contrast, biological echoes usually change smoothly [20, 21].
- Precipitation and biology have different vertical distributions. Most of the aerial animals concentrate into several heights where their flight is aided by the wind. The vertical structure of precipitation echoes is more complicated [22].

Figure 2 shows vertical slices of the precipitation and biological echoes, and the typical measured data of their reflectivity factor products. The above-described four differences between the precipitation and biological echoes are visible in the diagrams (Figure 2(a) and (b)). Owing to these differences, the weather radar PPI scans of precipitation and biology are clearly distinguishable by humans (Figure 2(c) and (d)). More specifically, (i) the higher echo top of precipitation than biology widens the coverage of precipitation in the PPI scans, especially at higher elevations; (ii) the maximum dBZ is much higher for precipitation echoes than for biological echoes (45 dBZ vs. 20 dBZ); (iii) precipitation echoes exhibit a coarser texture than biological echoes; and (iv) the precipitation scans expand with elevation whereas the

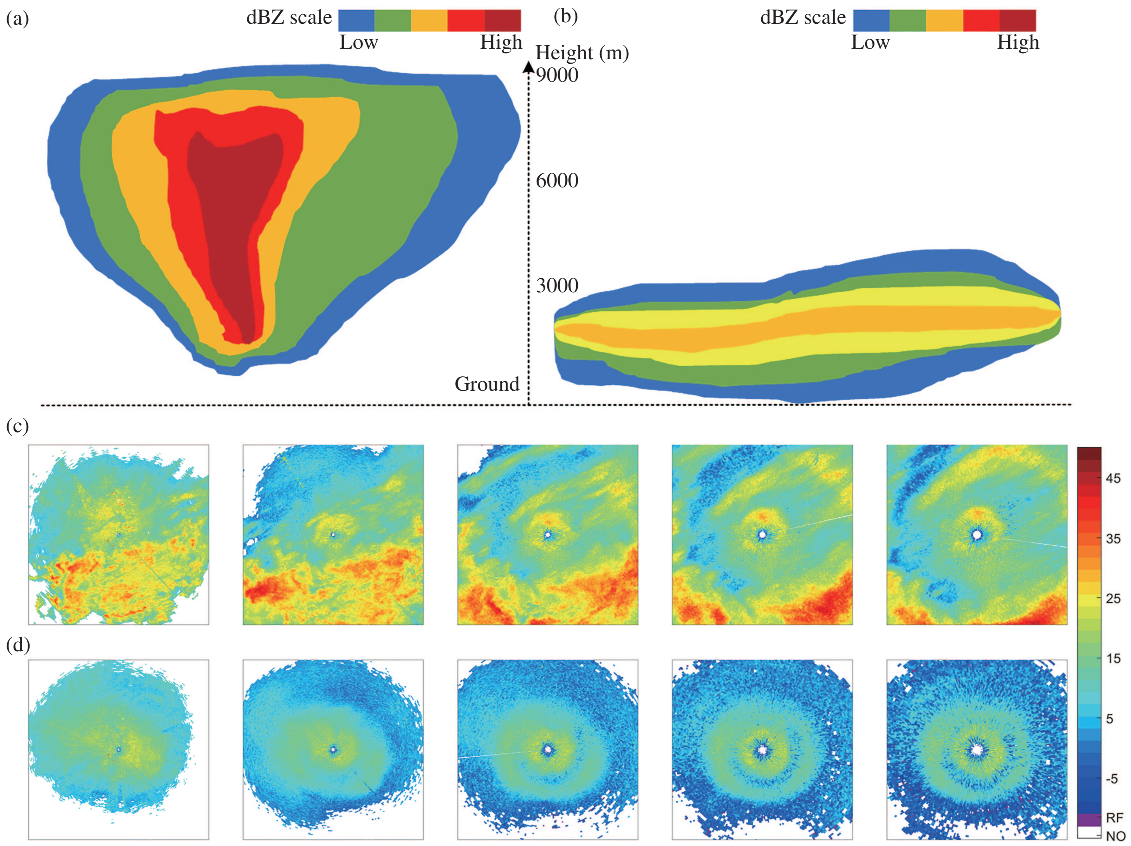

Figure 2 (Color online) (a) and (b) Vertical slices of precipitation and biological echoes. (c) and (d) Typical reflectivity factor products of precipitation and biology deduced from the Xuzhou weather radar station. (c) 12:13 UTC on September 27th and (d) 11:41 UTC on August 31st, 2017. Echo types are confirmed by checking the historical weather conditions. From left to right, the subgraphs are scanned at elevations of 0.5°, 1.45°, 2.4°, 3.35°, and 4.3°, with plotting radii of 227, 127, 81, 58 and 45 km, respectively. These radii correspond to a height range of 3000 m (bottom limit of the antenna beam).

biological scans are almost unchanged because the targets are concentrated in particular height ranges and are widely distributed.

As demanded by the extraction module input, we linearly map the radar reflectivity factor data at each elevation onto a 0 to 255 scale (here, we select the range −15 dBZ to 50 dBZ to cover most of the data) and cast them into Cartesian grid images (of resolution 321 by 321 to fit the extraction module). Following a previous study [12], we choose the lowest five elevation data in each data file and render them into five grayscale images. After these operations, the polar grid reflectivity factor data are converted to grayscale-image inputs for the extraction module.

2.2 Biological echo extraction

The biological echo extraction process aims to obtain the biological echoes and remove the precipitation echoes. To discriminate the biological and precipitation phenomena in the radar data, we transform the extraction procedure into an image segmentation task, which assigns semantic labels to every pixel in an image. The biological echo extraction process is overviewed in Figure 3. After mapping and rendering, the gray scale image enters the neural network, which is trained for image segmentation. The network output is used as a mask that filters out the precipitation and retains the biological echoes.

2.2.1 *Dataset description*

To train and evaluate the segmentation network, we must build up a dataset of weather radar biological echoes. Because most operational weather radars in China are singly polarized, no additional information

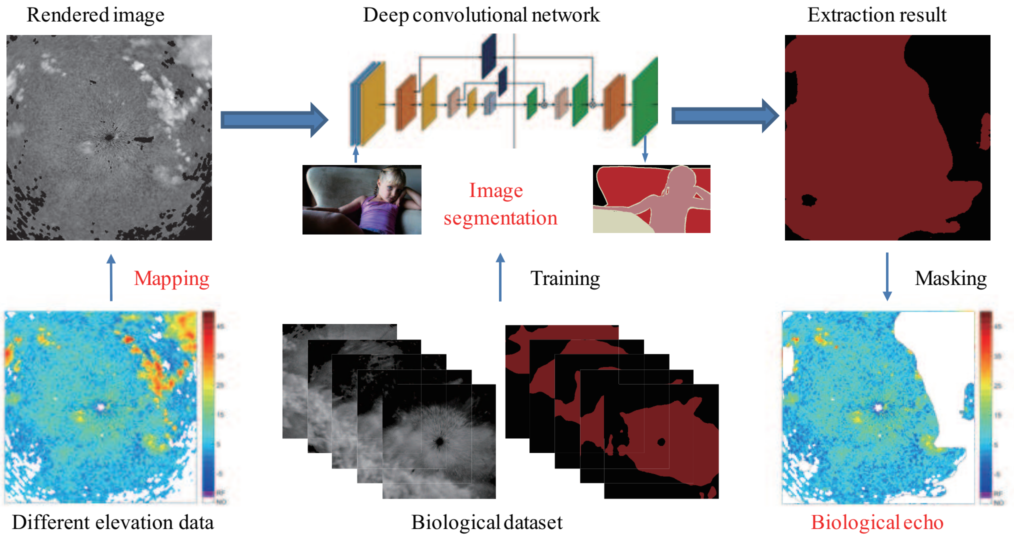

Figure 3 (Color online) Biological echo extraction process. The weather radar data are mapped to grayscale images by a linear mapping method. The biological dataset contains 1500 images for training the convolutional network at each elevation.

is available for annotations. Assisted by MATLAB® R2017a image segmenter app, we manually label 1500 images (300 images at each of the lowest five elevations). These scans are randomly selected from all Chinese weather radar stations from August 2017 through May 2018. Prior to the experiments, the labeled images are split into training and evaluation subsets (250 images for training and 50 images for evaluation at each elevation).

2.2.2 *Segmentation network*

In image segmentation tasks, deep CNNs show promising improvements over methods relying on hand-crafted features. A deep neural network transforms an input image into output values through a sequence of linear and nonlinear transformations. When appropriately structured, the network (like humans) learns experiences from both local and global information. It also determines the proper key features through the training process, requiring no artificial intervention to affect the decision process. For this purpose, we employ the DeepLabv3+ model because it attains state-of-the-art performance and its structure captures the contextual information on multiple scales [23].

To effectively locate the required biological areas, we train five semantic segmentation networks with the same structure. We then segment the biological areas of the five lowest-elevation radar data. Figure 4 overviews our modified DeepLabv3+ model. Our segmentation networks are based on the DeepLabv3+ model with the following modifications.

- We reduce the input image size to 321 by 321 to match the radar data and to reduce the GPU memory consumption. For better exploiting the multi-scale information, we also reduce the rates of the parallel atrous convolution (called atrous spatial pyramid pooling, or ASPP). Specifically, the output resolution of a deep CNN structure is 1/16 of the input resolution. The deep CNN output resolution of the original structure is 33 by 33 for a 513 by 513 image, and the ASPP atrous rates are 6, 12 and 18. The deep CNN output resolution of the modified structure is 21 by 21 and the atrous rates are reduced to 4, 8 and 12.
- We reduce the decoder output stride to 1 for densifying the output feature map. We forward the upsample operation to the front of the concatenation operation and change the upsample rate of the high-level features to 16. Thus, the two 3 by 3 convolution layers with 256 filters at the end of the decoder have the same resolution as the input images. Thereby, the decoder module could refine the segmentation results along the object boundaries.

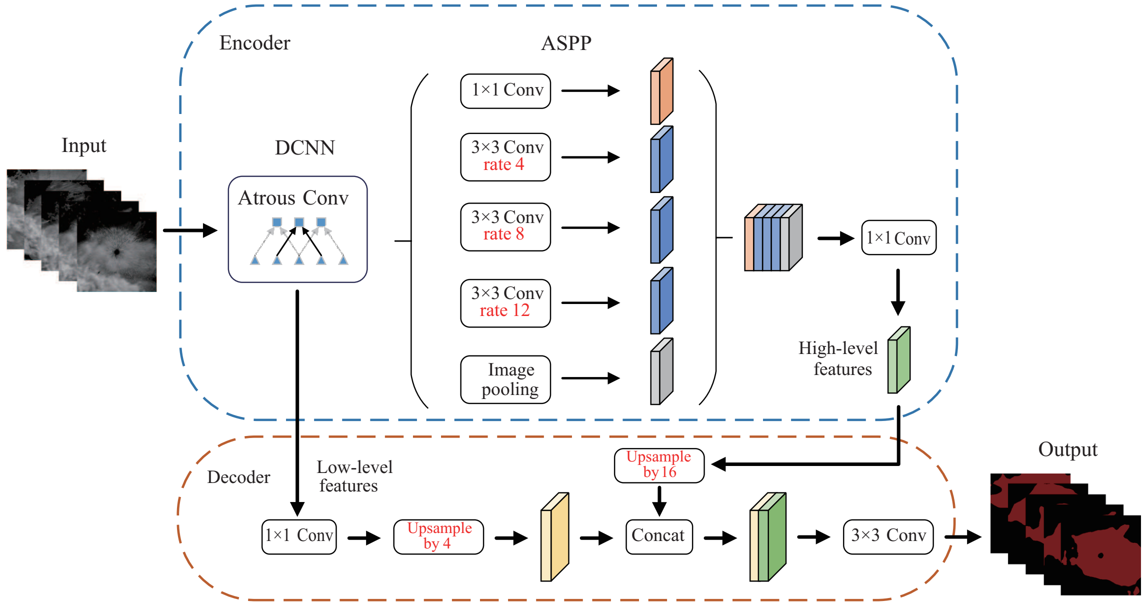

Figure 4 (Color online) DeepLabv3+-based network for extracting the biological information from weather radar. The input resolution is 321 by 321 and the atrous rates in the ASPP part are correspondingly reduced to 6, 8 and 12. The decoder output stride is reduced to 1 for densifying the output feature map.

2.2.3 *Experiments*

In preliminary experiments, the image segmentation model is evaluated on the prepared dataset discussed above. It is found that: (i) the image segmentation model achieves acceptable performance while reducing the manual labor; (ii) the pixel accuracies at all elevations exceed 92%; (iii) the modified structure improves the mean intersection-over-union (mIOU) by approximately 0.77% on average.

In our experiment, Xception is employed as the network backbone and the crop size is set to 321 by 321 for memory efficiency. Rather than creating the training data from scratch, we train our weather radar data segmentation model on checkpoints that are pretrained on Pascal VOC 2012 [24]. Although these color images largely differ from our grayscale weather radar images, both image types have similar characteristics of their low-level features. The pretrained model can greatly reduce the time consumption of training and avoid the risk of model non-convergence. After training the ASPP and decoder weights in the experiments, we accelerate the training by re-using the network backbone weights. To evaluate the improvement of our modification, we train the original and modified structures using the same training protocol and calculate their segmentation performances. In each training process, we apply a 'poly' policy with an initial learning rate of 0.0007 and a learning power of 0.9 over 160 epochs. The training process is completed in approximately 25 min. Experiments are implemented on the deep learning framework Tensorflow [25] and execute on a workstation with two Intel® 14-core Xeon E5 CPUs with 256 GB RAM and four Nvidia® GTX-1080Ti GPUs with 11 GB memory. The operating system is Windows® Server 2016.

Figure 5 shows the training losses and sample segmentation results at each elevation. The training process is checked on tensorboard. The training losses rapidly decrease after approximately 200 steps and finally converge. The segmentation results confirm that the trained model can recognize biological echoes and discriminate them from precipitation. The model performances at each elevation are assessed by the pixel accuracies and mIOU values. These performance metrics are summarized in Table 1. At all elevations, the pixel accuracies and mIOUs exceed 92% and 85%, respectively. Averaged over the five elevations, the pixel accuracies and mIOU metrics of the segmentation are 0.43% and 0.77% higher, respectively, in our modified models than in the original DeepLabv3+ structures. Given the small training dataset (1500 labeled images) and training time (several hours), these results are eminently satisfactory.

Next, we compare the performance metrics of our method with those of MistNet [12]. The results

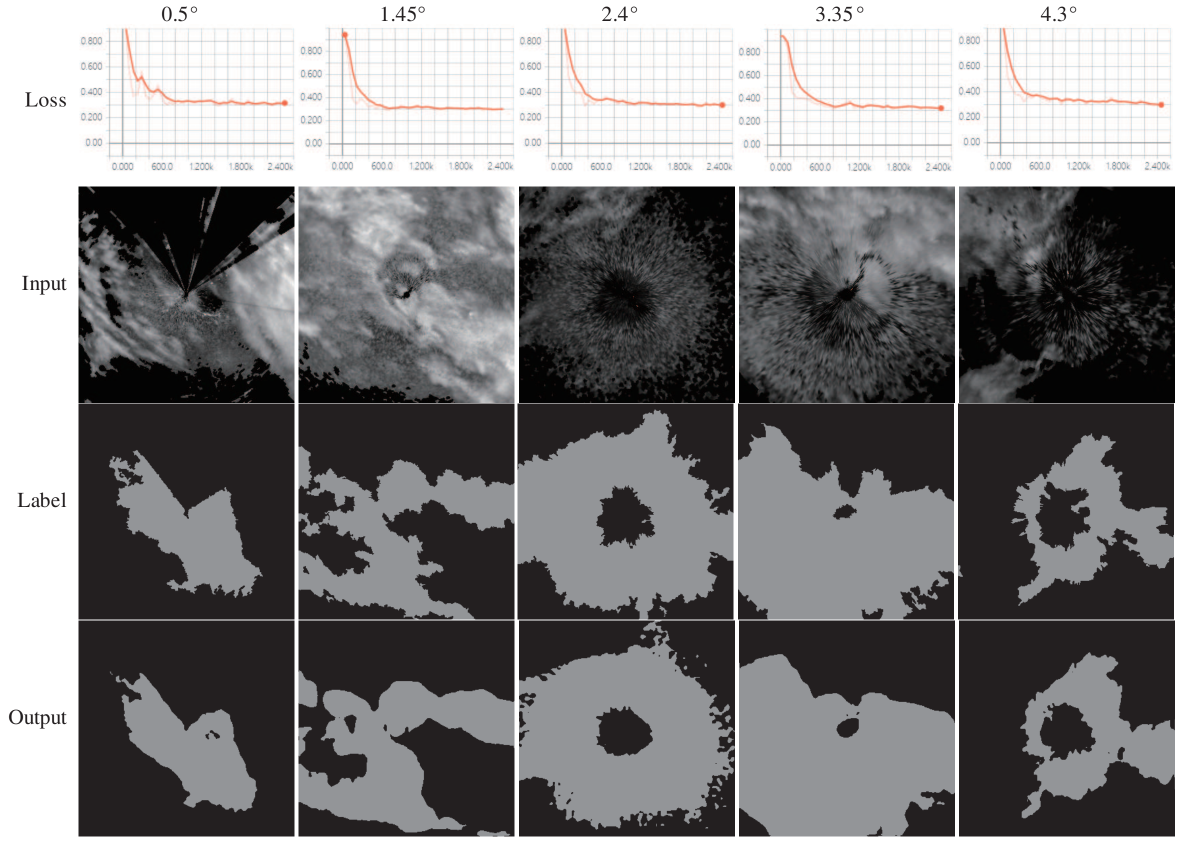

Figure 5 (Color online) Training losses and typical segmentation results of the training dataset at each elevation. The training losses are recorded as functions of the number of training steps. The input images are rendered and casted from the weather radar data. The brightness of the input images is linearly related to the radar reflectivity factor. The label images are manually constructed using the MATLAB image segmentation app. The output images are the segmentation results of the trained models. In the label and output images, the black and gray pixels represent the non-biological and biological areas, respectively.

Table 1 Segmentation performance at each elevation

Elevation	Pixel accuracy		mIOU	
	Original (%)	Ours (%)	Original (%)	Ours (%)
0.5°	94.80	95.30	89.85	90.81
1.35°	95.59	95.53	91.28	91.94
2.4°	92.63	93.04	86.19	86.91
3.35°	92.02	92.37	85.19	85.78
4.3°	91.76	92.29	84.59	85.51

Table 2 Performance comparison between our method and a previous work

Method	Precision (%)	Recall (%)	F-score (%)
Ours	92.6	92.4	92.5
MistNet	72.6	96.1	82.7

are shown in Table 2. In this table, the performance metrics of our method are averaged over the five elevations, and those of MistNet are evaluated on the 'Historical (weather)' dataset, whose size and echo compositions are most similar to ours. Our method outperforms MistNet in terms of the precision and F-score, confirming that our method better handles situations involving weather echoes than the previous work.

By combining the radar data rendering procedure and the biological extraction procedure, we obtain the biological echo masks. Using these masks, we filter out the precipitation echoes and retain the

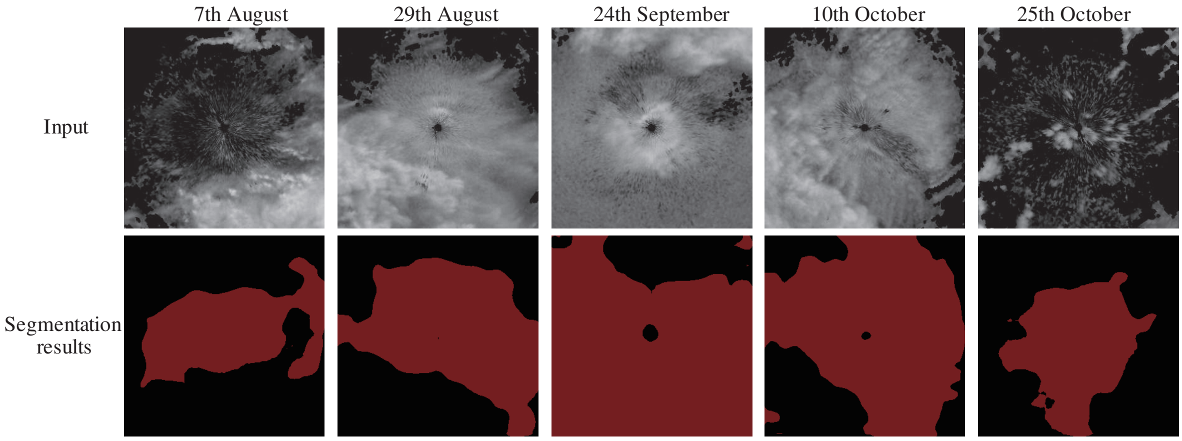

Figure 6 (Color online) Typical extraction results on different dates. The images in the first row are acquired at an elevation angle of 2.4°, and the brightness is linearly related to the radar reflectivity factor. The images in the second row are the segmentation results of the trained model at the third elevation angle. Biological echoes are found in the red areas.

biological information.

3 Demonstration

This section demonstrates our proposed method in two cases. First, we analyze the biogeographical patterns in typical weather radar obtained from an operational radar located on the migration route of insects and birds. Second, we attempt to analyze the large-scale migration pattern from multiple weather radars.

3.1 Typical extraction results

To validate and test the proposed method, we collect and process additional weather radar data. The Xuzhou radar station (34.3°N, 117.2°E) is chosen as a typical data source for validation because it locates on the migration route and the geographical condition is suitable for radar observations. Figure 6 shows the segmentation results of the selected stations on different dates. For simplicity, we present only the results obtained at the third elevation angle. In these typical extraction results, the precipitation echoes (found in the bottom areas of the 7th and 29th August patterns, the upper area of the 24th September pattern, and the lower left part of the 10th October pattern) are successfully recognized as non-biological echoes. In addition, the intensity and coverage area of the biological echo first increases and then decreases as the dates progress, consistent with the regular pattern of autumn migrations.

3.2 Large-scale migration pattern

To reveal the large-scale migration pattern, we collect and process the data of more than 90 radar stations collected on two typical migration dates in China: one in spring, the other in autumn. We first gather the data and extract the biological echoes by the proposed modified network as described in Figure 3. Second, we convert the biological echoes at each station to a relative quantity (the instantaneous migration intensity) by summing the reflectivity factors within the radar domain. Third, we calculate the target mean airspeed and direction from the corresponding radial velocity using the velocity-azimuth display technique [26]. Finally, to interpret the geological features, we visualize these large-scale migration results on a map.

The large-scale migration patterns obtained by the proposed method are shown in Figure 7. A typical nocturnal migration pattern is revealed. The animals migrate northeast in spring and southwest in autumn.

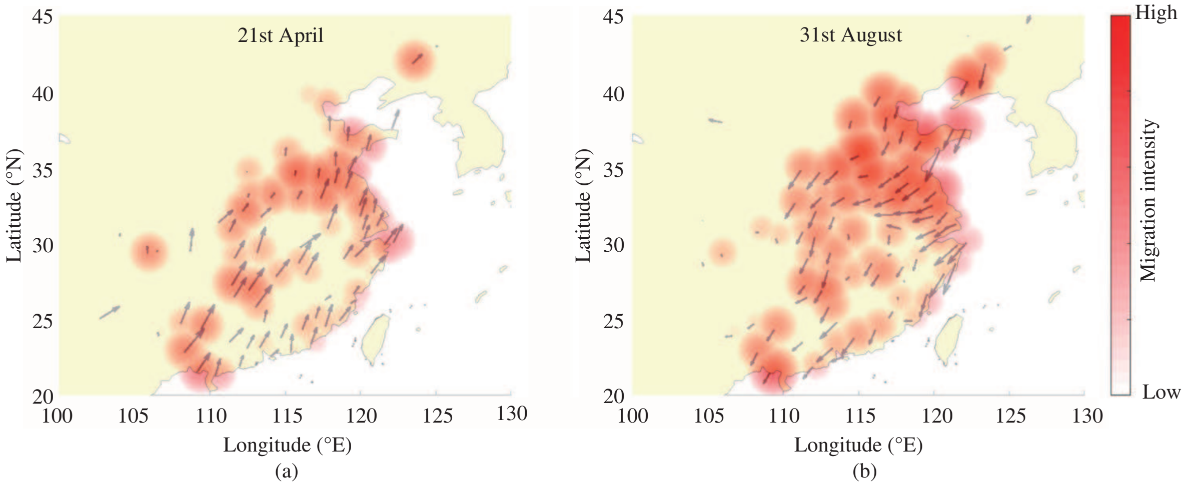

Figure 7 (Color online) Large-scale migration pattern in China. (a) Spring; (b) autumn. The red color bar represents the relative migration intensity calculated from the segmentation results (a high red concentration denotes intense migration). The sizes and directions of the arrow represent the average airspeeds and directions, respectively, of the targets passing the radar station. All data are collected at 21:00 local time.

4 Conclusion

We proposed a method that extracts biological information from weather radar. The method is based on the weather radar observation geometry and applies an image segmentation technique. In two typical animal-movement cases, we demonstrated the possibility of extracting local-scale and large-scale biological phenomena from Chinese weather radar network data.

Acknowledgements This work was supported by National Natural Science Foundation of China (Grant No. 31727901). The authors thank Prof. Kongming WU, Dr. Qiulin WU and Haowen ZHANG, Institute of Plant Protection, Chinese Academy of Agricultural Sciences, for their kindly discussion and useful suggestions. The authors thank Dongli WU and Dasheng YANG, Meteorological Observation Center, China Meteorological Administration, for providing Chinese weather radar data.

References

1 van Doren B M, Horton K G. A continental system for forecasting bird migration. Science, 2018, 361: 1115–1118
2 Kelly J F, Horton K G. Toward a predictive macrosystems framework for migration ecology. Glob Ecol Biogeogr, 2016, 25: 1159–1165
3 Chilson P B, Frick W F, Stepanian P M, et al. Estimating animal densities in the aerosphere using weather radar: to Z or not to Z? Ecosphere, 2012, 3: 1–19
4 Rosenberg K V, Dokter A M, Blancher P J, et al. Decline of the North American avifauna. Science, 2019, 366: 120–124
5 Hu C, Cui K, Wang R, et al. A retrieval method of vertical profiles of reflectivity for migratory animals using weather radar. IEEE Trans Geosci Remote Sens, 2020, 58: 1030–1040
6 Stepanian P M, Horton K G. Extracting migrant flight orientation profiles using polarimetric radar. IEEE Trans Geosci Remote Sens, 2015, 53: 6518–6528
7 Hu C, Kong S, Wang R, et al. Identification of migratory insects from their physical features using a decision-tree support vector machine and its application to radar entomology. Sci Rep, 2018, 8: 5449
8 Hu C, Li W, Wang R, et al. Accurate insect orientation extraction based on polarization scattering matrix estimation. IEEE Geosci Remote Sens Lett, 2017, 14: 1755–1759
9 Hu C, Li W Q, Wang R, et al. Insect flight speed estimation analysis based on a full-polarization radar. Sci China Inf Sci, 2018, 61: 109306
10 Hu C, Wang Y X, Wang R, et al. An improved radar detection and tracking method for small UAV under clutter environment. Sci China Inf Sci, 2019, 62: 029306
11 Krizhevsky A, Sutskever I, Hinton G E. Imagenet classification with deep convolutional neural networks. In: Proceedings of the 25th International Conference on Neural Information Processing Systems, 2012. 1097–1105
12 Lin T Y, Winner K, Bernstein G, et al. MistNet: measuring historical bird migration in the us using archived weather radar data and convolutional neural networks. Methods Ecol Evol, 2019, 10: 1908–1922
13 Hu C, Li S, Wang R, et al. Extracting animal migration pattern from weather radar observation based on deep convolutional neural networks. J Eng, 2019, 93: 6541–6545

14 Chilson C, Avery K, McGovern A, et al. Automated detection of bird roosts using NEXRAD radar data and convolutional neural networks. Remote Sens Ecol Conserv, 2019, 5: 20–32
15 Xu X F. Construction, techniques and application of new generation doppler weather radar network in China. Eng Sci, 2004, 1: 15–25
16 Zhu X, Zhu J. New generation weather radar network in China (in Chinese). Meteorolog Sci Tech, 2004, 32:
17 Lakshmanan V, Hondl K, Potvin C K, et al. An improved method for estimating radar echo-top height. Wea Forecast, 2013, 28: 481–488
18 Bruderer B, Liechti F. Variation in density and height distribution of nocturnal migration in the south of Israel. Israel J Zoology, 2013, 41: 477–487
19 Rennie S J, Curtis M, Peter J, et al. Bayesian echo classification for Australian single-polarization weather radar with application to assimilation of radial velocity observations. J Atmos Ocean Technol, 2015, 32: 1341–1355
20 Zhang P, Liu S, Xu Q. Identifying Doppler velocity contamination caused by migrating birds. part i: feature extraction and quantification. J Atmos Ocean Technol, 2005, 22: 1105–1113
21 Lakshmanan V, Fritz A, Smith T, et al. An automated technique to quality control radar reflectivity data. J Appl Meteor Climatol, 2007, 46: 288–305
22 Hu G, Lim K S, Horvitz N, et al. Mass seasonal bioflows of high-flying insect migrants. Science, 2016, 354: 1584–1587
23 Chen L C, Zhu Y, Papandreou G, et al. Encoder-decoder with atrous separable convolution for semantic image segmentation. In: Proceedings of the European Conference on Computer Vision (ECCV), 2018. 801–818
24 Everingham M, Eslami S M A, van Gool L, et al. The pascal visual object classes challenge: a retrospective. Int J Comput Vis, 2015, 111: 98–136
25 Abadi M, Agarwal A, Barham P, et al. Tensorflow: large-scale machine learning on heterogeneous distributed systems. 2016. ArXiv: 1603.04467
26 Browning K A, Wexler R. The determination of kinematic properties of a wind field using doppler radar. J Appl Meteor, 1968, 7: 105–113